RESEARCH

A radiomics model utilizing CT for the early detection and diagnosis of severe community-acquired pneumonia

Jia Jiang[1†], Siqin Chen[1†], Shaofeng Zhang[1†], Yaling Zeng[1], Jiayi Liu[1], Wei lei[1], Xiang Liu[2*], Xin Chen[3*] and Qiang Xiao[1,3*]

Abstract

Background Community-Acquired Pneumonia (CAP) remains a significant global health concern, with a subset of cases progressing to Severe Community-Acquired Pneumonia (SCAP). This study aims to develop and validate a CT-based radiomics model for the early detection of SCAP to enable timely intervention and improve patient outcomes.

Methods A retrospective study was conducted on 115 CAP and SCAP patients at Southern Medical University Shunde Hospital from January to December 2021. Using the Pyradiomics package, 107 radiomic features were extracted from CT scans, refined via intra-class and inter-class correlation coefficients, and narrowed down using the Least Absolute Shrinkage and Selection Operator (LASSO) regression model. The predictive performance of the radiomics-based model was assessed through receiver operating characteristic (ROC) analysis, employing machine learning classifiers such as k-Nearest Neighbors (KNN), Support Vector Machine (SVM), Logistic Regression (LR), and Random Forest (RF), trained and validated on datasets split 7:3, with a training set ($n = 80$) and a validation set ($n = 35$).

Results The radiomics model exhibited robust predictive performance, with the RF classifier achieving superior precision and accuracy compared to LR, SVM, and KNN classifiers. Specifically, the RF classifier demonstrated a precision of 0.977 (training set) and 0.833 (validation set), as well as an accuracy of 0.925 (training set) and 0.857 (validation set), suggesting its superior performance in both metrics. Decision Curve Analysis (DCA) was utilized to evaluate the clinical efficacy of the RF classifier, demonstrating a favorable net benefit within the threshold ranges of 0.1 to 0.8 for the training set and 0.2 to 0.7 for the validation set.

[†]Jia Jiang, Siqin Chen and Shaofeng Zhang contributed equally to this work.

*Correspondence:
Xiang Liu
angu870751@163.com
Xin Chen
chen_xin1020@163.com
Qiang Xiao
xiaoqiang@smu.edu.cn

Full list of author information is available at the end of the article

Conclusions The radiomics model developed in this study shows promise for early SCAP detection and can improve clinical decision-making.

Keywords CT, Radiomics features, Severe community-acquired pneumonia, Detection and diagnosis

Introduction

Community-acquired pneumonia (CAP) continues to exhibit high incidence and mortality rates, leading to frequent instances of misdiagnosis and inappropriate treatment [1]. The progression to severe community-acquired pneumonia (SCAP) is associated with a significant increase in mortality, which remains elevated despite intensive care unit (ICU) intervention [2]. SCAP is a grave infectious disease originating in the lungs, with the potential for rapid advancement to respiratory failure. Patients with SCAP necessitating mechanical ventilation as a result of septic shock may experience a mortality rate surpassing 35%, whereas individuals developing acute respiratory distress syndrome (ARDS) exhibit a mortality rate exceeding 30% [3]. Those who survive often endure long-term consequences, including impaired lung function, diminished neurological and cognitive capacities, and limited mobility [4]. Timely recognition of SCAP, facilitating prompt and appropriate intervention, has the potential to enhance patient prognoses and mitigate the development of these sequelae. Early identification of SCAP patients is imperative for prompt and precise treatment, as well as for preventing delays in critical care, ultimately leading to a reduction in mortality rates [5, 6].

Imaging techniques are essential in the field of medicine due to their non-invasive nature, which assists in clinical decision-making [7]. Chest CT scans are considered valuable tools for diagnosing pneumonia, assessing its severity, and evaluating the efficacy of treatment [8, 9]. The imaging features commonly associated with CAP consist of patchy infiltrates, air bronchograms, and interlobular septal thickening. Conversely, SCAP typically presents with widespread pulmonary consolidation and bilateral lung involvement [10, 11]. Nevertheless, these characteristics are not always distinct, and the shared imaging features of CAP and SCAP can complicate differentiation based solely on manual interpretation of computed tomography (CT) images. And the interpretation of clinical images is often hindered by the subjective nature of physicians' analysis, which is heavily reliant on their experience. Simple visual inspection often falls short of the needs of precision medicine and individualized treatment. Therefore, decoding and quantitatively presenting macroscopic information from images is crucial for clinical decision-making, treatment planning, and prognostic assessment.

Radiomics, first proposed by Lambin et al. [12]. in 2012, is a novel approach to medical image analysis that involves the extraction of quantitative features from images in a high-throughput manner. By comparing radiomic features with clinical data, radiomics facilitates the diagnosis and prognosis of diseases [12, 13]. In recent years, there has been a growing utilization of radiomics for the assessment and detection of pneumonia lesions [14]. This trend has been particularly notable in light of the worldwide scarcity of medical professionals during the COVID-19 pandemic, leading to increased interest in the utilization of computer-based medical image processing technology for pneumonia diagnosis. The primary focus of radiomics in pneumonia diagnosis lies in the differentiation of COVID-19 and Viral Pneumonia, pneumonia-like lung cancer, and checkpoint inhibitor-related pneumonitis [15–17]. Radiomics is predominantly utilized in the diagnosis, staging, prognosis, and prediction of tumor responses in lung diseases. Recent research has shown the emerging potential of radiomics in diagnosing pneumonia, assessing its severity, and evaluating prognosis [15, 18–21]. These studies suggest that radiomics features have the potential to serve as imaging biomarkers for predicting clinical outcomes and prognoses.
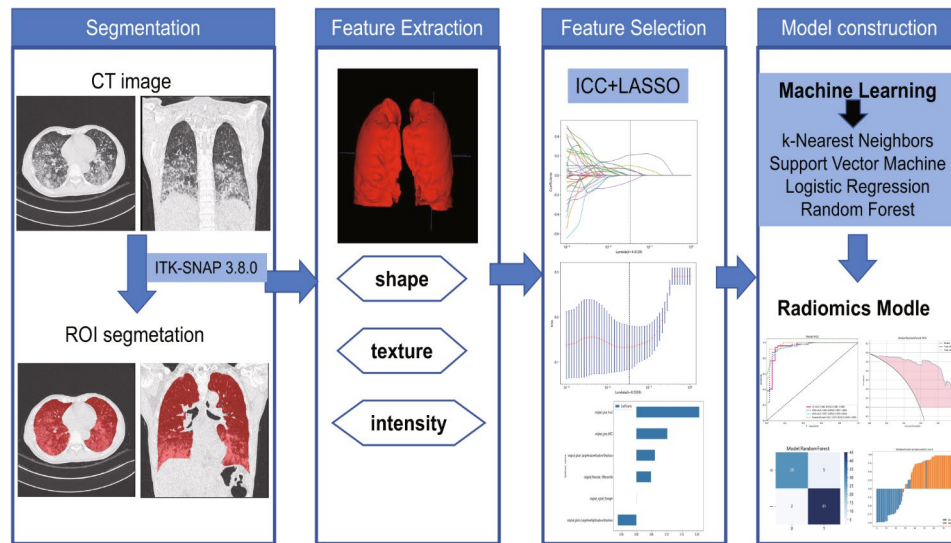
The objective of this study is to create a prognostic model for the severity of CAP using CT radiomics analysis, which may facilitate early identification of severe cases and improve patient outcomes through prompt intervention. The results of this research show significant potential for the progression of precision medicine and the improvement of personalized treatment strategies.

Materials and methods
Patients
In this retrospective study, a total of 115 cases diagnosed with CAP and SCAP between January and December 2021 at Shunde Hospital of Southern Medical University were analyzed. The specific inclusion criteria included meeting the diagnostic criteria for CAP or SCAP [22–24], having clear lung CT images within three days of admission, and possessing comprehensive clinical baseline information. The specific exclusion criteria included lack of CT images within 3 days, hospital infections and unclear CT images. In this study, patients were randomly allocated into two cohorts, with a ratio of 7:3, identified as the training and testing cohorts. The patient enrollment process is illustrated in Fig. 1. Approval for this retrospective study was obtained from the Ethics Committee of Shunde Hospital of Southern Medical University. All procedures adhered to the Declaration of Helsinki and pertinent regulations in China.

Fig. 1 The flow chart depicted in this study outlines the process of enrolling patients, including the selection and allocation of study subjects. A total of 115 patients were ultimately included, with 80 assigned to the training set and 35 to the validation set at a ratio of 7:3. The flow chart and main text provide comprehensive details regarding the specific criteria for inclusion and exclusion of patients

Imaging acquisition and segmentation

The imaging of all patients was conducted using a 128-detector row CT scanner (SIEMENS SOMATOM Definition Flash-CT scanner; Siemens, Erlangen, Germany) with specific parameters: reconstruction slice thickness of 0.6 mm, acquisition field of view (FOV) of 300 mm, beam pitch of 1.2, collimation width of 64×0.625 mm, matrix of 512×512, tube voltage of 120 kV, and tube current of 200 mA. Patients were instructed to hold their breath to minimize motion-related artifacts during imaging. The resulting images were captured using lung window settings with a width of 1600 HU and a level of -600 HU. Prior to segmenting lung lobes and lesions, the images underwent normalization by adjusting grayscale values with a scale factor of 1000 and were resampled to an isotropic voxel size of $3 \times 3 \times 3$ mm³ using nearest neighbor interpolation. Additionally, an additional padding distance of 10 mm was implemented to address large sigma values in the Laplacian of Gaussian (LoG) filtering process. The intensity values were discretized using a fixed bin width of 5 Hounsfield Units (HU).

CT images were obtained from the Picture Archiving and Communication System (PACS) for the purpose of analyzing diffuse lung lesions in SCAP cases. The entire lung tissue was delineated for examination. Subsequently, two radiologists, each with 5 and 10 years of experience, respectively, utilized ITK-SNAP software (version 3.8.0) for the manual delineation of central lesion areas within three-dimensional Regions of Interest (ROI). These ROI were then carefully reviewed by a third radiologist with 15 years of experience in the field.

Radiomics workflow

Figure 2 delineates the radiomics workflow, comprising five essential stages: (1) delineation of ROI, (2) extraction of radiomics features, (3) selection of radiomics features, (4) construction of the prediction model using a training dataset, and (5) evaluation of the prediction model's efficacy. This sequential process elucidates a methodical framework for the examination of radiographic images, beginning with initial segmentation and culminating in the assessment of model performance. Each stage plays a pivotal role in guaranteeing the precision and dependability of the radiomics analysis.

Radiomics feature extraction and selection

The radiomic features were extracted utilizing Pyradonis's proprietary feature analysis program (http://pyradiomics. readthedocs.io). The extraction process encompassed a variety of radiomics features, including first-order statistics, the Grey Level Co-occurrence Matrix (GLCM), the Gray Level Dependence Matrix (GLDM), the Grey Level Run-Length Matrix (GLRLM), the Gray Level Size Zone Matrix (GLSZM), the neighborhood gray-tone difference matrix (NGTDM), and shape features.

In order to enhance the efficiency of our analysis, we implemented two techniques to systematically eliminate redundant features. The selection of intra- and inter-class correlation coefficients (ICC) was utilized to evaluate

Jiang *et al. BMC Medical Imaging*   (2024) 24:202

Page 4 of 11

Fig. 2 Workflow of radiomic analysis in this study. Nodules were segmented by radiologists, and features were extracted and selected by LASSO based on which the prediction model, DCA, Decision curve analysis, confusion matrices and sample prediction waterfall charts

and preserve highly reproducible characteristics, thereby ensuring consistency across various imaging conditions. The LASSO method was employed for its capacity to conduct variable selection and regularization concurrently, thereby reducing dimensionality while retaining the most predictive features [25]. This approach guarantees the inclusion of solely statistically significant and pertinent features in our model. The patient radiomic features were initially standardized using z-score normalization. ICC was calculated for each radiomic feature, with those exceeding 0.9 selected for further analysis. LASSO model was then employed to further reduce the dimensionality of the feature set and identify the most important features. The optimal lambda value for the LASSO model was determined through a tenfold cross-validation process within the training set.

Radiomics model construction and validation
This study involved the development of radiomics-based models utilizing four classifiers: KNN, SVM, LR, and RF. These models were created by combining selected radiomics features with the aforementioned classifiers. The performance of the models was evaluated using the area under the curve (AUC) from ROC analysis, and a 95% confidence interval (CI) was provided for the results. DCA was performed to assess the clinical utility of the model by determining the net benefit across various threshold probabilities for both the training and test datasets. The Confusion Matrix outlined the true and false positives/negatives, yielding metrics such as accuracy and sensitivity. Sample Prediction Histograms visually depicted the model's prediction confidence, highlighting potential biases. Collectively, these analyses evaluated

the model's diagnostic efficacy in identifying SCAP and informed strategies for enhancing its reliability.

Statistical analysis and experimental parameters
Statistical analysis was performed utilizing Python and SPSS 25.0. Categorical variables were presented as frequencies and percentages. The normality of continuous variables was evaluated through Kolmogorov-Smirnov or Shapiro-Wilk tests. Quantitative data were presented as mean±standard deviation or median (interquartile range). Disparities between subgroups were examined using t-tests or Mann-Whitney U tests for continuous variables, and Chi-square tests for categorical variables. Statistical significance was established at $p<0.05$ (two-tailed). In this research, the hyperparameters employed for the machine learning models were as follows: A Random Forest model was utilized with 10 trees, minimum samples split of 2, and a random state of 0. The Support Vector Machine was configured to provide probability estimates with a random state of 0. The K-Nearest Neighbors algorithm utilized the "kd tree" method. The Logistic Regression model had a random state of 0.

The experiments were carried out utilizing a system equipped with a 13th Generation Intel(R) Core (TM) i5-13500 H processor running at 2.60 GHz, 32 GB of RAM, Intel(R) Iris(R) Xe Graphics, and a 954 GB SSD. Image processing and radiomics feature extraction were executed using Python (version 3.8) along with various libraries such as Pydicom, SimpleITK, PyRadiomics, Matplotlib, Seaborn, Pandas, Scikit-learn, among others.

Results

Patients characteristics

This research, which included 115 patients diagnosed with CAP and SCAP who met the designated inclusion and exclusion criteria, was carried out between January and December of 2021. Following a randomization ratio of 7:3, the patients were divided into a training set ($n=80$) and a validation set ($n=35$). Analysis within the training set revealed no significant differences between the two diseases in terms of age, gender, smoking status, sputum production, chest pain, fatigue, diabetes and kidney disease. Significant associations were observed between fever, cough and hypertension with the type of disease ($p<0.05$). In the validation set, factors including age, gender, smoking, fever, cough, sputum, chest pain, fatigue, hypertension, diabetes and kidney disease did not show significant differences between CAP and SCAP. A detailed description of the baseline characteristics of the patients can be found in Table 1.

Radiomics feature extraction and selection

In our study, a total of 115 ROI were analyzed. Utilizing the Pyradiomics package, 107 radiomic features were extracted, encompassing 18 first-order features, 24 Gy Level Coherence Matrix (GLCM) features, 14 Gy Level Dependence Matrix (GLDM) features, 16 Gy Level Run Length Matrix (GLRLM) features, 16 Gy Level Size Zone Matrix (GLSZM) features, 5 Neighboring Gray Tone Difference Matrix (NGTDM) features, and 14 shape features. The selection of radiomics features involved calculating intra-class and ICC for each extracted feature.

Features with an ICC exceeding 0.9 were deemed highly correlated, resulting in the retention of only one feature and a reduction of the significant image features to 38. Following this, relevant features were identified through the application of the LASSO regression model and a forward selection approach, as illustrated in Fig. 3a. The optimal performance of the LASSO regression, characterized by a penalty parameter of 0.0339, led to the attainment of the smallest mean squared error. Based on the LASSO regression analysis depicted in Fig. 3b, the optimized hyperparameter λ was determined to be 0.0339, leading to the preservation of six radiomic features. These features consist of original firstorder 10 Percentile, original glcm Imc2, original glcm MCC, original glszm Large Area High Gray Level Emphasis, original glszm Large Area Low Gray Level Emphasis, and original_ngtdm_Strength. Consequently, six radiomic features along with their corresponding feature weights were identified (Fig. 3c).

### Model establishment and evaluation

ROC analysis was employed to evaluate the predictive performance of radiomic-based models (Fig. 4). Within the training set, the AUC values for the KNN, SVM, LR, and RF models were 0.957, 0.954, 0.943, and 0.975, respectively. In the validation set, the overall AUC values for KNN, SVM, LR, and RF were 0.909, 0.956, 0.969, and 0.888, respectively. Furthermore, the study found promising results in terms of accuracy, sensitivity, and specificity for the KNN, SVM, LR, and RF classifiers, as outlined in Table 2. Out of the four classifier models examined, the

Table 1 Comparison of severity and clinical characteristics in both training and validation cohort

Characteristic	Training cohort($n=80$)			Validation cohort($n=35$)		
	nsCAP($n=43$)	SCAP($n=47$)	*p* value	nsCAP($n=22$)	SCAP($n=13$)	*p* value
Age(year)	68(50,73)	65.49±13.507	0.381	60±21.463	68.08±13.041	0.175
Gender						
Male	17(51.5%)	32(68.1%)	0.134	12(54.5%)	10(76.9%)	0.282
Female	16(48.5%)	15(31.9%)		10(45.5%)	3(23.1%)	
Smoke						
Yes	8(24.2%)	21(44.7%)	0.061	8(36.4)	3(23.1)	0.478
No	25(75.8%)	26(55.3%)		14(63.6%)	10(76.9%)	
Symptoms						
Fever	20(60.6%)	41(87.2%)	0.006*	12(54.5%)	11(84.6%)	0.139
Cough	30(90.9%)	34(72.3%)	0.041*	21(95.5%)	10(76.9%)	0.134
Sputum	24(72.7%)	31(66%)	0.52	17(77.35)	9(69.2%)	0.698
Chest pain	5(15.2%)	3(6.4%)	0.364	1(4.5%)	0(0%)	1
Fatigue	12(36.4%)	26(55.3%)	0.095	4(18.2%)	5(38.5%)	0.243
Underlying disease						
HBP	11(33.3%)	28(59.6%)	0.021*	12(54.5%)	10(76.95%)	0.282
DM	4(12.1%)	11(23.4%)	0.203	5(22.7%)	3(23.1%)	1
Chronic kidney disease	3(9.1%)	5(10.6%)	1	1(4.5%)	3(23.1%)	0.134

Quantitative data were presented as mean±standard deviation or median (interquartile range). Count data were presented as number (%). *nsCAP* Non-severe community-acquired pneumonia, *SCAP* Severe community-acquired pneumonia, *HBP* High blood pressure, *DM*, Diabetes mellitus *Indicates a significant value, *P*<0.05
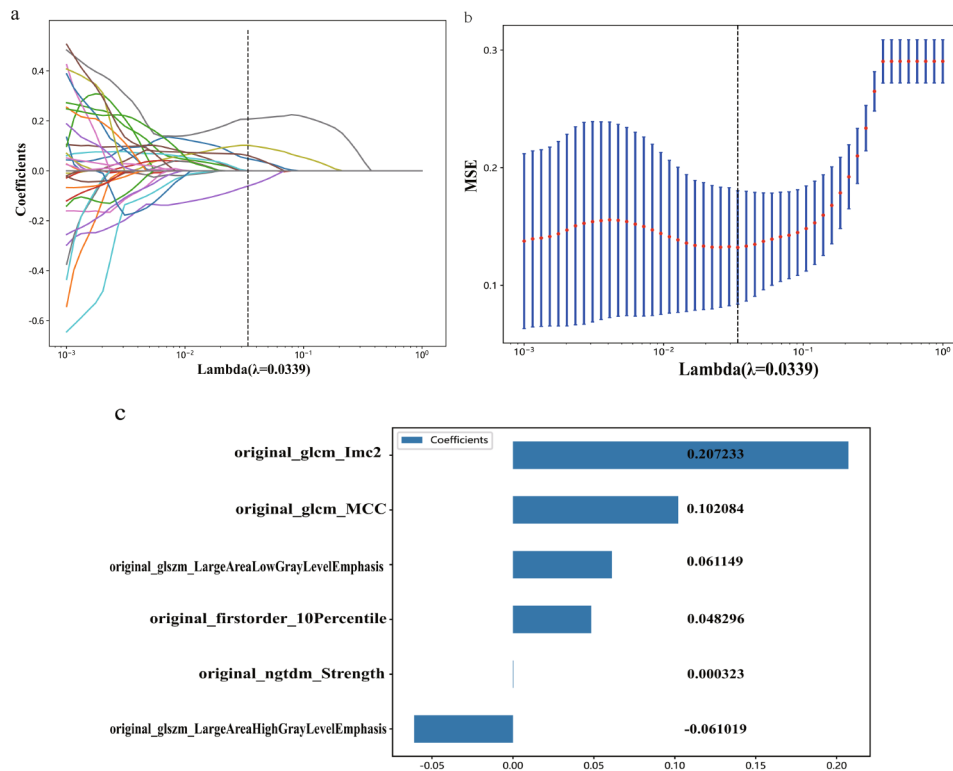
Fig. 3 Radiomic feature selection based on LASSO algorithm. **a**, **b** Ten-fold cross-validated coefficients and 10-fold cross-validated MSE. **c** The histogram of the Rad score based on the selected features
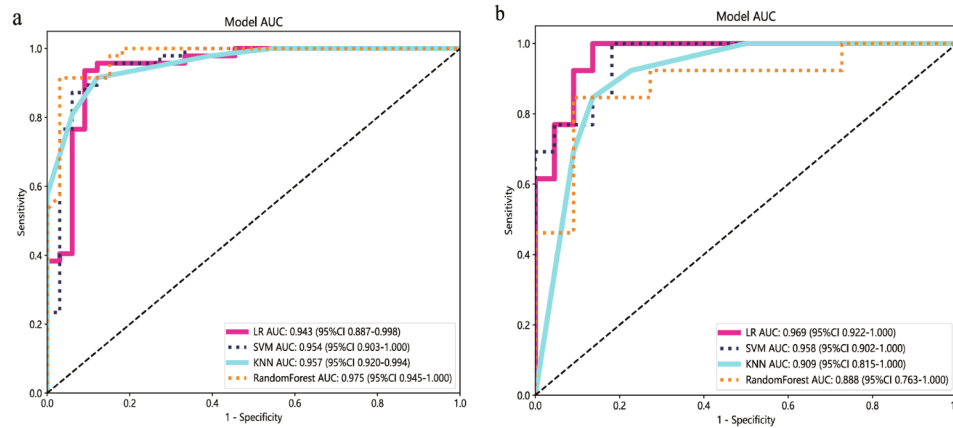
Fig. 4 Comparison of Receiver Operating Characteristic (ROC) curves for the four classifiers on both the training (**a**) and testing cohorts (**b**)

Table 2 Diagnostic efficiency of different models in the training cohort and testing cohort

Model name	Accuracy	AUC	95% CI	Sensitivity	Specificity	PPV	NPV	Precision
LR(Training set)	0.912	0.943	0.8870–0.9982	0.915	0.909	0.935	0.882	0.935
LR(Testing set)	0.886	0.969	0.9217–1.0000	0.923	0.864	0.8	0.95	0.8
SVM(Training set)	0.887	0.954	0.9028–1.0000	0.851	0.939	0.952	0.816	0.952
SVM(Testing set)	0.857	0.958	0.9022–1.0000	0.923	0.818	0.75	0.947	0.75
KNN(Training set)	0.863	0.957	0.9196–0.9940	0.809	0.939	0.95	0.775	0.95
KNN(Testing set)	0.829	0.909	0.8150–1.0000	0.692	0.909	0.818	0.833	0.818
RandomForest(Training set)	0.925	0.975	0.9452–1.0000	0.894	0.97	0.977	0.865	0.977
RandomForest(Testing set)	0.857	0.888	0.7629–1.0000	0.769	0.909	0.833	0.87	0.833

LR Logistic regression, *SVM* Support vector machine, *KNN* K-Nearest neighbor, *AUC* Area under curve, *PPV* Positive predictive value, *NPV*, Negative predictive value

RF classifier demonstrated superior precision and accuracy. In particular, the RF classifier exhibited an accuracy of 0.977 on the training set and 0.833 on the validation set, as well as precision scores of 0.925 for the training set and 0.857 for the validation set. These performance metrics outperformed those of the other classifier models. DCA was employed to assess the clinical utility of the RF classifier. The findings of the analysis indicate that the RF classifier yielded a favorable net benefit within the specified threshold intervals of 0.1 to 0.8 for the training set and 0.2 to 0.7 for the validation set, underscoring its efficacy in informing clinical decision-making (Fig. 5a and b). Additionally, confusion matrices and sample prediction waterfall charts were utilized to showcase the predictive capabilities of the models, as depicted in Fig. 6a, b, c, and d. The model's performance in distinguishing between patients with CAP and SCAP was assessed through the utilization of a confusion matrix. Additionally, sample waterfall prediction charts were utilized to illustrate the model's confidence levels in predicting individual samples, with notable instances of high confidence observed in certain predictions. These analyses collectively demonstrate the efficacy of our radiomics model in accurately identifying SCAP patients at an early stage.

Discussion

Due to the swift advancement and elevated fatality rate associated with CAP, the timely evaluation of disease progression is imperative. The early detection of patients afflicted with SCAP has the potential to greatly enhance treatment approaches and patient prognoses [26–28]. In this research, we showcased the effectiveness of CT imaging attributes by constructing radiomic models utilizing quantitative imaging characteristics across four classifier methodologies. The efficacy of the models was confirmed through the utilization of ROC curves, DCA, confusion matrices, and sample prediction waterfall charts. The findings indicate that the model is capable of accurately distinguishing between CAP and SCAP in the initial stages, underscoring the significant predictive

utility of radiomic features extracted from CT images for timely detection of SCAP.

Numerous assessment tools exist for evaluating the severity of pneumonia, with the Pneumonia Severity Index (PSI) and the CURB-65 score emerging as prevalent metrics [29, 30]. While the PSI is renowned for its robust prognostic capabilities in predicting mortality, its intricate nature presents obstacles to routine implementation in clinical practice [31]. CURB-65 exhibits comparatively lower sensitivity, particularly in the prediction of admissions to the Intensive Care Unit (ICU) [32]. Both the Pneumonia Severity Index (PSI) and CURB-65 rely on clinical symptoms, standard laboratory indices, and radiological findings. However, the initial phases of the disease may manifest with nonspecific symptoms, ambiguous laboratory indicators, and subjective evaluations of radiological findings by radiologists, posing challenges in the timely and accurate diagnosis of SCAP [31]. As a result, there remains a persistent demand for improved assessment techniques in clinical settings. The diagnosis of CAP requires the presence of an infiltrate, as visualized on imaging modalities such as chest X-ray, chest CT scan, or lung ultrasonography, in individuals exhibiting symptoms consistent with the disease [33]. CT scans are particularly valuable due to their high sensitivity in detecting CAP early and identifying complications in certain patient populations [34]. They play a crucial role in offering detailed insights into the location, severity, and features of pneumonia. Therefore, radiological examinations play a crucial role in evaluating the severity of CAP. The etiology of CAP is diverse, including bacterial, viral, and mycoplasma infections, all of which can contribute to the onset of CAP. Various pathogens may present with different radiological features, with SCAP often exhibiting diffuse pulmonary lesions [35]. This article presents a radiomic model for the early detection of SCAP using CT based on specific premises. The model is designed to identify SCAP by segmenting the entire lung volume and extracting 6 radiomic features. The study's methodology uses quantitative imaging feature analysis to eliminate the subjectivity of manual CT image interpretation.
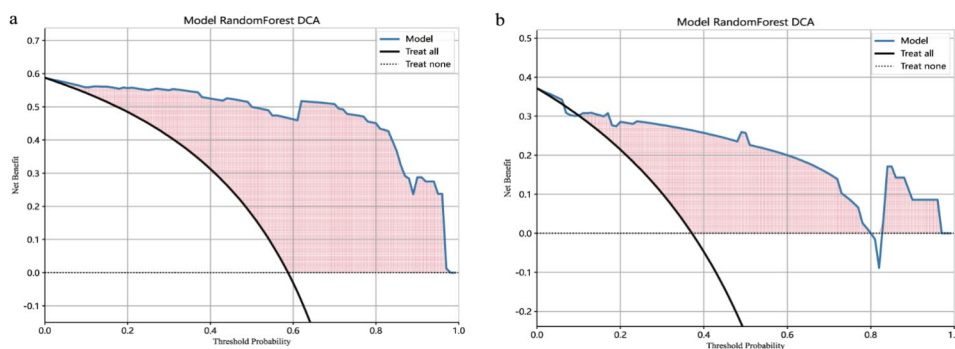
Fig. 5 Decision curves of the training (**a**) and testing cohorts (**b**)
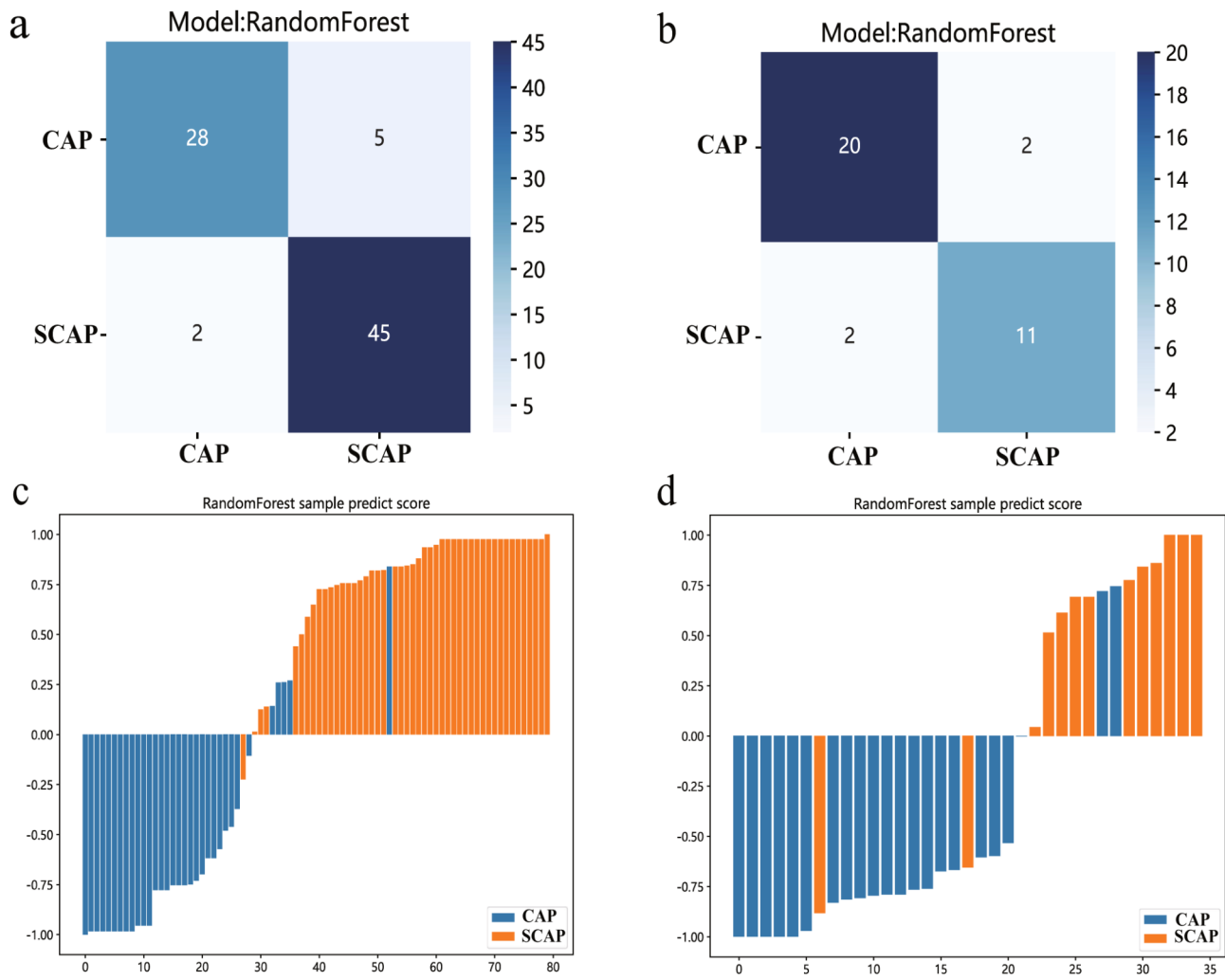
Fig. 6 Confusion matrices and sample prediction waterfall charts of the training (**a**, **c**) and testing cohorts (**b**, **d**)

Radiomics, a quantitative imaging analysis technique, is commonly utilized in clinical research for the purposes of early detection, prognosis, and predicting treatment response [36, 37]. This method involves extracting quantitative data from images to identify phenotypic differences and correlating them with clinical information [38, 39]. The radiomics process consists of four stages: image acquisition, image segmentation, feature extraction, and informatics analysis. Radiomics features are classified according to shape and size, texture derived from filtered images, fractal properties, image intensity histograms, and the interrelationships among image voxels [40, 41]. Subsequent to feature extraction, dimensionality reduction methods such as ICC and LASSO regression are employed to identify significant features. Subsequently, Machine Learning (ML) classifiers are utilized for disease classification and prediction [41]. In this research, the entire volume of both lungs was contoured, and the ROI for each patient was manually segmented by a physician with expertise in lung CT imaging. Through the

use of radiological features' ICC and LASSO regression, the study reduced 107 imaging features to 6. Following this, four classifiers, namely KNN, SVM, LR, and RF, were employed to construct radiomics-based models for the detection of SCAP. The findings of this study suggest that the four models evaluated exhibited strong predictive capabilities in feature classification methods, with accuracy exceeding 0.80 and AUC exceeding 0.85. This research highlights the potential of radiomics as a computer-assisted tool for extracting important biomedical data from CT images, which could aid in the early detection and treatment of SCAP. These results provide novel insights into the utilization of established radiomics and machine learning methodologies for improving pneumonia diagnosis.

Recently, radiomics has shown promise in the detection, severity assessment, and prognostic evaluation of pneumonia. Li et al. [18]. utilized radiomic features extracted from chest CT scans to develop a multivariable logistic regression model that incorporates both radiomic

and clinical data, successfully distinguishing between mycoplasma pneumonia and bacterial pneumonia. In the evaluation of pneumonia severity, it has been suggested that radiomic models utilizing CT features may serve as a valuable tool for prognosticating the severity of COVID-19 pneumonia, thereby potentially facilitating timely intervention strategies and mitigating mortality rates among COVID-19 patients [19]. Homayounieh et al. [42]. employed a comprehensive approach incorporating whole-lung radiomics, radiologist interpretations, and clinical variables to forecast pneumonia in individuals with COVID-19. Their findings indicate that radiomics holds greater significance compared to alternative diagnostic modalities. Radiomics features have shown a discriminative ability between outpatient and inpatient chest CTs, achieving an AUC of 0.84. Recent research, characterized by high accuracy and AUC values, suggests that radiomics analysis of whole-lung segmentation can effectively distinguish between confirmed cases of COVID-19 and suspected individuals [43–46]. The application of radiomics, a noninvasive, efficient, and cost-effective technique, has been expanded to assess the severity of CAP, resulting in a decrease in unnecessary interventions and alleviation of patient distress, especially in settings with limited resources. Once the model is developed, it can be smoothly incorporated into the CT interpretation software, streamlining the workflow for radiologists who need only delineate the entire lung volume, after which the system produces an objective outcome for their review. Existing literature indicates a dearth of research on the utilization of radiomics for evaluating the severity of CAP. This research develops a prognostic model for the severity of CAP using CT radiomics analysis, introducing an innovative method for the timely identification of SCAP. These findings have substantial implications for the progression of precision medicine and the enhancement of individualized and efficient treatment strategies.

Our research is constrained by several limitations. This retrospective study is subject to selection bias, and the manual delineation of Regions of Interest may introduce variability due to lesion irregularities. Moreover, it is important to note that this study was conducted at a single center with a sample size of 115 patients, which may limit the generalizability of the findings. The absence of an a priori power analysis underscores the necessity for future research to address this limitation. Moving forward, we recommend expanding sample sizes and incorporating data from multiple centers to improve the robustness and applicability of our model. Longitudinal follow-up studies are essential for validating the predictive efficacy of radiomics features in SCAP patients over time. Enhancing feature extraction and selection methods using advanced algorithms and machine learning techniques will enhance the predictive accuracy and interpretability of the model.

Conclusion

In this study, the radiomics model based on CT imaging have good performance in early identification of SCAP. The implications of our findings in the clinical setting are significant, as timely and precise identification of SCAP has the potential to enhance patient outcomes and streamline resource allocation within healthcare facilities. Implementation of this model in clinical practice can empower healthcare professionals to make evidence-based decisions, ultimately enhancing patient care and treatment. At the same time, it will provide new ideas for the research, diagnosis, and treatment of other types of pneumonia.

Data availability
The datasets used and analyzed during the current study are available from the corresponding author on reasonable request.

Declarations

Ethics approval and consent to participate
This study was approved by the local ethics committee of Shunde Hospital of Southern Medical University and the informed consent requirement was waived. All methods were carried out in accordance with relevant guidelines and regulations.

Consent for publication
Not applicable.

Competing interests
The authors declare no competing interests.

Author details
[1]Pulmonary and Critical Care Medicine, Shunde Hospital, Southern Medical University (The First People's Hospital of Shunde Foshan), No.1, Jiazi Road, Lunjiao Street, Shunde District, Foshan, Guangdong 528300, China
[2]Departments of Hematology, Shunde Hospital, Southern Medical University (The First People's Hospital of Shunde Foshan), No.1, Jiazi Road, Lunjiao Street, Shunde District, Foshan, Guangdong 528300, China

Jiang *et al. BMC Medical Imaging*   (2024) 24:202

Page 10 of 11

[3]Pulmonary and Critical Care Medicine, Zhujiang Hospital, Southern Medical University, 253 Gongye Middle Avenue, Haizhu District, Guangzhou, Guangdong 510280, China

References

1. Mandell LA. Community-acquired pneumonia: an overview [J]. Postgrad Med. 2015;127(6):607–15.
2. Nair GB, Niederman MS. Updates on community acquired pneumonia management in the ICU [J]. Pharmacol Ther. 2021;217:107663.
3. Niederman MS, Torres A. Severe community-acquired pneumonia [J]. *European respiratory review: an official journal of the European Respiratory Society*. 2022; 31(166).
4. Bein T, Weber-Carstens S, Apfelbacher C. Long-term outcome after the acute respiratory distress syndrome: different from general critical illness? [J]. Curr Opin Crit Care. 2018;24(1):35–40.
5. Woodhead M, Welch CA, Harrison DA, et al. Community-acquired pneumonia on the intensive care unit: secondary analysis of 17,869 cases in the ICNARC Case Mix Programme database [J]. Crit Care (London England). 2006;10(Suppl 2):S1.
6. Phua J, Ngerng WJ, Lim TK. The impact of a delay in intensive care unit admission for community-acquired pneumonia [J]. Eur Respir J. 2010;36(4):826–33.
7. Aerts HJ, Velazquez ER, Leijenaar RT, et al. Decoding tumour phenotype by noninvasive imaging using a quantitative radiomics approach [J]. Nat Commun. 2014;5:4006.
8. Debray MP, Carette MF, Loubet P, et al. CT features of community-acquired pneumonia at the emergency department [J]. Respiratory Med Res. 2022;81:100892.
9. Zu ZY, Jiang MD, Xu PP, et al. Coronavirus Disease 2019 (COVID-19): a perspective from China [J]. Radiology. 2020;296(2):E15–25.
10. Tanaka N, Emoto T, Suda H, et al. Community-acquired pneumonia: a correlative study between chest radiographic and HRCT findings [J]. Japanese J Radiol. 2015;33(6):317–28.
11. Franquet T, Chung JH Imaging of Pulmonary Infection [M]//HODLER J, KUBIK-HUCH R A. VON SCHULTHESS G K. Diseases of the Chest, Breast, Heart and Vessels 2019–2022: Diagnostic and Interventional Imaging. Cham; Springer International Publishing. 2019: 65–77.
12. Lambin P, Rios-Velazquez E, Leijenaar R et al. Radiomics: extracting more information from medical images using advanced feature analysis [J]. *European journal of cancer (Oxford, England*: 1990). 2012; 48(4): 441–446.
13. Lambin P, Leijenaar RTH, Deist TM, et al. Radiomics: the bridge between medical imaging and personalized medicine [J]. Nat Reviews Clin Oncol. 2017;14(12):749–62.
14. Lynch DA. Quantitative computed tomography of diffuse lung disease [J]. J Thorac Imaging. 2013;28(5):264–5.
15. Kao YS, Lin KT. A Meta-analysis of computerized tomography-based Radiomics for the diagnosis of COVID-19 and viral pneumonia [J]. Diagnostics (Basel Switzerland). 2021; 11(6).
16. Gong JW, Zhang Z, Luo TY, et al. Combined model of radiomics, clinical, and imaging features for differentiating focal pneumonia-like lung cancer from pulmonary inflammatory lesions: an exploratory study [J]. BMC Med Imaging. 2022;22(1):98.
17. Huang J, Chen X, Xia B, et al. Advances in CT features and radiomics of checkpoint inhibitor-related pneumonitis: a short review [J]. Front Immunol. 2023;14:1082980.
18. Li H, Li T, Cai Q et al. Development and validation of a Radiomics Nomogram for differentiating Mycoplasma Pneumonia and bacterial pneumonia [J]. Diagnostics (Basel Switzerland). 2021; 11(8).
19. Kao YS, Lin KT. A meta-analysis of the diagnostic test accuracy of CT-based radiomics for the prediction of COVID-19 severity [J]. Radiol Med. 2022;127(7):754–62.
20. Chen Z, Li X, Li J, et al. A COVID-19 risk score combining chest CT radiomics and clinical characteristics to differentiate COVID-19 pneumonia from other viral pneumonias [J]. Aging. 2021;13(7):9186–224.
21. Duan L, Zhang L, Lu G et al. A CT-Based Radiomics Model for Prediction of Prognosis in patients with Novel Coronavirus Disease (COVID-19) pneumonia: a preliminary study [J]. Diagnostics (Basel Switzerland). 2023; 13(8).
22. Mandell LA, Wunderink RG, Anzueto A, et al. Infectious Diseases Society of America/American Thoracic Society consensus guidelines on the management of community-acquired pneumonia in adults [J]. Clin Infect Diseases: Official Publication Infect Dis Soc Am. 2007;44(Suppl 2):S27–72.
23. Metlay JP, Waterer GW, Long AC, et al. Diagnosis and treatment of adults with community-acquired Pneumonia. An Official Clinical Practice Guideline of the American Thoracic Society and Infectious Diseases Society of America [J]. Am J Respir Crit Care Med. 2019;200(7):e45–67.
24. Cao B, Huang Y, She DY, et al. Diagnosis and treatment of community-acquired pneumonia in adults: 2016 clinical practice guidelines by the Chinese Thoracic Society, Chinese Medical Association [J]. Clin Respir J. 2018;12(4):1320–60.
25. Tibshirani R. Regression shrinkage and Selection Via the Lasso [J]. J Roy Stat Soc: Ser B (Methodol). 2018;58(1):267–88.
26. Lim HF, Phua J, Mukhopadhyay A, et al. IDSA/ATS minor criteria aid pre-intensive care unit resuscitation in severe community-acquired pneumonia [J]. Eur Respir J. 2014;43(3):852–62.
27. Frenzen FS, Kutschan U, Meiswinkel N et al. Admission lactate predicts poor prognosis independently of the CRB/CURB-65 scores in community-acquired pneumonia [J]. *Clinical microbiology and infection: the official publication of the European Society of Clinical Microbiology and Infectious Diseases*. 2018; 24(3): 306.e301–306.e306.
28. Kolditz M, Ewig S, Klapdor B, et al. Community-acquired pneumonia as medical emergency: predictors of early deterioration [J]. Thorax. 2015;70(6):551–8.
29. Fine MJ, Auble TE, Yealy DM, et al. A prediction rule to identify low-risk patients with community-acquired pneumonia [J]. N Engl J Med. 1997;336(4):243–50.
30. Lim WS, van der Eerden MM, Laing R, et al. Defining community acquired pneumonia severity on presentation to hospital: an international derivation and validation study [J]. Thorax. 2003;58(5):377–82.
31. Singanayagam A, Chalmers JD, Hill AT. Severity assessment in community-acquired pneumonia: a review [J]. QJM: Monthly J Association Physicians. 2009;102(6):379–88.
32. Kaal AG, Op de Hoek L, Hochheimer DT et al. Outcomes of community-acquired pneumonia using the Pneumonia Severity Index versus the CURB-65 in routine practice of emergency departments [J]. ERJ open Res. 2023; 9(3).
33. Moore M, Stuart B, Little P et al. Predictors of pneumonia in lower respiratory tract infections: 3 C prospective cough complication cohort study [J]. Eur Respir J. 2017; 50(5).
34. Aliberti S, Dela Cruz CS, Amati F, et al. Community-acquired pneumonia [J]. Lancet (London England). 2021;398(10303):906–19.
35. Franquet T. Imaging of community-acquired pneumonia [J]. J Thorac Imaging. 2018;33(5):282–94.
36. Mayerhoefer ME, Materka A, Langs G, et al. Introduction to Radiomics [J]. J Nuclear Medicine: Official Publication Soc Nuclear Med. 2020;61(4):488–95.
37. Liu P, Gu Q, Hu X, et al. Applying a radiomics-based strategy to preoperatively predict lymph node metastasis in the resectable pancreatic ductal adenocarcinoma [J]. J X-Ray Sci Technol. 2020;28(6):1113–21.
38. Rizzo S, Botta F, Raimondi S, et al. Radiomics: the facts and the challenges of image analysis [J]. Eur Radiol Experimental. 2018;2(1):36.
39. Gillies RJ, Kinahan PE, Hricak H. Radiomics: images are more than pictures, they are data [J]. Radiology. 2016;278(2):563–77.
40. Parekh V, Jacobs MA. Radiomics: a new application from established techniques [J]. Expert Rev Precision Med drug Dev. 2016;1(2):207–26.
41. Erickson BJ, Korfiatis P, Akkus Z, et al. Machine learning for medical imaging [J]. Radiographics: Rev Publication Radiological Soc North Am Inc. 2017;37(2):505–15.
42. Homayounieh F, Ebrahimian S, Babaei R, et al. CT Radiomics, radiologists, and Clinical Information in Predicting Outcome of patients with COVID-19 pneumonia [J]. Radiol Cardiothorac Imaging. 2020;2(4):e200322.
43. Fu L, Li Y, Cheng A, et al. A Novel Machine Learning-derived Radiomic signature of the whole lung differentiates stable from progressive COVID-19 infection: a retrospective cohort study [J]. J Thorac Imaging. 2020;35(6):361–8.
44. Rezaeijo SM, Abedi-Firouzjah R, Ghorvei M, et al. Screening of COVID-19 based on the extracted radiomics features from chest CT images [J]. J X-Ray Sci Technol. 2021;29(2):229–43.
45. Zorzi G, Berta L, Rizzetto F, et al. Artificial intelligence for differentiating COVID-19 from other viral pneumonias on CT: comparative analysis of different models based on quantitative and radiomic approaches [J]. Eur Radiol Experimental. 2023;7(1):3.

46. Wu S, Zhang R, Wan X, et al. Chest computed tomography radiomics to predict the outcome for patients with COVID-19 at an early stage [J]. Diagn Interv Radiol (Ankara Turkey). 2023;29(1):91–102.

Publisher's Note